Physics Letters B 782 (2018) 619–626

Contents lists available at ScienceDirect

Physics Letters B

www.elsevier.com/locate/physletb

# Nuclear moments of the low-lying isomeric $1^+$ state of $^{34}$Al: Investigation on the neutron $1p1h$ excitation across $N = 20$ in the island of inversion

Z.Y. Xu [a,*], H. Heylen [a,b,c,*], K. Asahi [d,e], F. Boulay [f], J.M. Daugas [f], R.P. de Groote [a,1], W. Gins [a], O. Kamalou [g], Á. Koszorús [a], M. Lykiardopoulou [h,2], T.J. Mertzimekis [h], G. Neyens [a,b,*], H. Nishibata [d], T. Otsuka [i,j,k,a], R. Orset [f], A. Poves [l], T. Sato [d], C. Stodel [g], J.C. Thomas [g], N. Tsunoda [i], Y. Utsuno [m,i], M. Vandebrouck [g,n], X.F. Yang [a,3]

[a] KU Leuven, Instituut voor Kern- en Stralingsfysica, Celestijnenlaan 200D, 3001 Leuven, Belgium
[b] Experimental Physics Department, CERN, CH-1211 Geneva 23, Switzerland
[c] Max-Planck-Institut fur Kernphysik, D-69117 Heidelberg, Germany
[d] RIKEN Nishina Center, 2-1 Hirosawa, Wako, Saitama 351-0198, Japan
[e] Department of Physics, Tokyo Institute of Technology, Meguro, Tokyo 152-8551, Japan
[f] CEA, DAM, DIF, F-91297 Arpajon Cedex, France
[g] GANIL, CEA/DRF-CNRS/IN2P3, B.P. 55027, F-14076 Caen Cedex 5, France
[h] Department of Physics, University of Athens, Zografou Campus, GR-15784, Athens, Greece
[i] Center for Nuclear Study, University of Tokyo, 7-3-1 Hongo, Bunkyo-ku, Tokyo, Japan
[j] Department of Physics, University of Tokyo, 7-3-1 Hongo, Bunkyo-ku, Tokyo, Japan
[k] National Superconducting Cyclotron Laboratory, Michigan State University, East Lansing, MI, 48824, USA
[l] Departamento de Física Teórica and IFT, UAM-CSIC, Universidad Autónoma de Madrid, E-28049 Madrid, Spain
[m] Advanced Science Research Center, Japan Atomic Energy Agency, Tokai, Ibaraki 319-1195, Japan
[n] Irfu, CEA, Université Paris-Saclay, 91191 Gif-sur-Yvette, France

ARTICLE INFO

*Article history:*
Received 9 February 2018
Received in revised form 2 April 2018
Accepted 6 June 2018
Available online 14 June 2018
Editor: V. Metag

*Keywords:*
$\beta$-NMR/NQR
$g$ factor
Quadrupole moment
$^{34m}$Al

ABSTRACT

The nuclear $g$ factor and quadrupole moment ($Q_s$) have been measured for the low-lying isomeric $1^+$ state of $^{34}$Al, using the $\beta$-detected nuclear magnetic resonance ($\beta$-NMR) and quadrupole resonance ($\beta$-NQR) methods. Spin-polarized $^{34}$Al isotopes were produced in a one-neutron pickup reaction induced by a $^{36}$S beam on a $^{9}$Be target at a kinetic energy of 77.5 MeV/nucleon, and were collected with the LISE fragment separator at GANIL. The measured $g$ factor ($|g|$ in a range of $1.757 \pm 0.014$) and quadrupole moment ($|Q_s| = 38(5)$ mb) are in good agreement with shell-model calculations using effective interactions. The similarity between the $g$ factor of $^{34m}$Al and that of $^{32}$Al confirms a dominant neutron $2p1h$ configuration $\pi(d_{5/2})^{-1} \otimes \nu(d_{3/2})^{-1}(f_{7/2})^2$ of $^{34m}$Al. In addition, the enhanced quadrupole moment of $^{34m}$Al relative to that of $^{32}$Al suggests that the neutron $1p1h$ excitation across the $N = 20$ shell gap introduces extra nucleon–nucleon correlation and deformation.



Thanks to the experimental techniques exploiting radioactive ion beams, exotic nuclei have been extensively produced and investigated in recent decades, bringing crucial challenges to nuclear-structure theories up to date. It has been revealed that even though the shell structure in stable nuclei can be well interpreted using simplified mean fields plus spin-orbit interactions [1,2], it may vary drastically in exotic nuclei due to the residual nucleon–nucleon interaction which produces different effective single particle energies depending on the proton-to-neutron ($Z/N$) ratio [3]. One of such typical examples is the $N = 20$ island of inversion [4], where unexpected ground-state deformation has been observed in the neutron-rich isotopes in the vicinity of $^{32}$Mg ($Z = 12$). The relevant anomalies were first discovered in 1975 in the binding

* Corresponding author.
*E-mail address:* zhengyu.xu@kuleuven.be (Z.Y. Xu).
[1] Current affiliation: Department of Physics, University of Jyväskylä, Survontie 9, FI-40014 Jyväskylä, Finland.
[2] Current affiliation: Department of Physics and Astronomy, University of British Columbia, 6224 Agricultural Road, Vancouver, BC V6T1Z1, Canada.
[3] Current affiliation: School of Physics and State Key Laboratory of Nuclear Physics and Technology, Peking University, Beijing 100871, China.

https://doi.org/10.1016/j.physletb.2018.06.009

energies of $^{31,32}$Na [5] and shortly afterwards extended to the charge radius of $^{31}$Na [6] and the low-lying $2^+$ state of $^{32}$Mg [7], indicating a strong ground-state deformation in spite of the neutron closed shell. Later, theoretical works using large-scale shell-model calculations associated this deformation with $2p2h$ excitations across $N = 20$, in which two neutrons are excited from the *sd* shell to the *pf* shell [4,8]. For isotopes belonging to the island of inversion, the energy of those $2p2h$ intruder configurations is lower than that of the normal configurations, giving rise to the deformed ground states. More recently, this remarkable phenomenon was understood as a general consequence of monopole-based changes in the spherical mean field and strong quadrupole correlations in exotic nuclei far from stability [9,10].

Following the pioneering work in 1970s, many experimental efforts have been devoted to examine the shell evolution near and inside the island of inversion [11–34]. While the ground states of Mg isotopes with $N \sim 20$ are dominated by intruder configurations [13,14,18,20,21,24], those of the Si isotopes are associated with normal *sd*-shell configurations, placing the $Z = 14$ isotopes outside the island of inversion [26]. As such, the Al isotopes ($Z = 13$) in between Mg and Si should be characterized by transitional behavior from normal to intruder configurations. Indeed, the ground-state $g$ factors and quadrupole moments up to $N = 19$ are nicely described by the shell-model calculations within the *sd* shell [35–38], whereas from $N = 20$ onwards the inclusion of the *pf* shell is crucial to reproduce the ground-state properties observed experimentally [22,39–41].

From the experimental point of view, the low-lying states of $^{34}$Al ($N = 21$) remain to be investigated more extensively. Even though the ground-state $g$ factor suggests a strong mixing of intruder ($2p2h$) and normal ($0p0h$) configurations in the ground state [22], mass measurements support the argument this is a normal-configuration state [34]. Besides, a low-lying $1^+$ state originating from $1p1h$ excitations across $N = 20$ was anticipated in $^{34}$Al by shell-model calculations using the SDPF-M interaction [22]. Due to the large spin gap between the $1^+$ state and the states underneath, the former is predicted to be an isomer. The first experimental evidence for this $1^+$ isomer (referred to in the following as $^{34m}$Al, to be distinguished from the ground state $^{34g}$Al) was observed indirectly in the $\beta$ decay of $^{34}$Al, feeding the intruder $0_2^+$ state of $^{34}$Si through a strong Gamow–Teller (GT) transition [42]. More recently, a systematic study on the low-lying states of $^{34}$Al was carried out via the $\beta$ decay of $^{34}$Mg, putting the isomer 46.6 keV above the ground $4^-$ state [43]. To pin down the microscopic configuration of this isomer unambiguously, its $g$ factor and quadrupole moment are indispensable. While the $g$ factor probes the orbital occupation of unpaired nucleons in a certain state, the quadrupole moment $Q$ is more sensitive to nuclear correlations and associated deformation [44]. Theoretically, the unpaired proton and neutron in $^{34m}$Al ($1^+$) occupy the same single-particle orbits as that in the $^{32}$Al $1^+$ ground state, therefore their $g$ factors should be similar. On the other hand, due to the intruder nature of the isomer, it may be more strongly deformed than the $^{32}$Al ground state, resulting in a larger quadrupole moment. More generally, measuring the $g$ factor and quadrupole moment of $^{34m}$Al helps to establish a unified picture of deformation and its underlying nucleon–nucleon interaction in the island of inversion as $^{34m}$Al is so far the only case in which the increase in deformation due to a $1p1h$ excitation can be experimentally investigated in a long-lived state.

This Letter reports on the first $g$-factor and quadrupole-moment measurements of the isomeric $1^+$ state of $^{34}$Al, using the continuous-beam $\beta$-NMR/NQR techniques. To investigate the configurations of the isomer, the results are compared to large-scale shell-model calculations with different effective interactions.

Spin-polarized $^{34}$Al ($N = 21$) isotopes were produced in the one-neutron pick-up reaction of a $^{36}S^{16+}$ ($N = 20$) beam (77.5 MeV/nucleon) on a 1-mm-thick $^9$Be target, similar to Ref. [45]. A $^{34}$Al beam with about 80% purity was obtained using the high-resolution fragmentation separator LISE at GANIL. The neutron-rich Al nuclei were transmitted to the $\beta$-NMR/NQR setup [46], where they were implanted into either a Si or a $\alpha$-$Al_2O_3$ crystal, depending on the observable ($g$ factor or $Q_s$) to be measured. The entire experimental setup was hold under vacuum at room temperature. To maintain the nuclear spin polarization, the crystal was placed in a static magnetic field $B_0$ ($\sim$1500 gauss) parallel to the spin orientation. A Helmholtz coil was mounted around the implantation crystal to generate a radio-frequency (rf) field of a few gauss perpendicular to the static field, with a frequency $\nu_{\mathrm{RF}}$. The $\beta$-decay asymmetry of polarized nuclei was recorded using two sets of $\Delta E$–$E$ plastic scintillator telescopes placed above and below the implantation crystal in the vacuum chamber. Coincidences between the $\Delta E$ and $E$ scintillators were made in each telescope to reduce the random background in our $\beta$-detection system. For a spin-polarized ensemble, the experimental $\beta$-decay asymmetry $\mathcal{A}$ is defined as

$$\mathcal{A} = \frac{N_{\mathrm{up}} - N_{\mathrm{down}}}{N_{\mathrm{up}} + N_{\mathrm{down}}} \approx Q_{\mathrm{exp}} A_\beta P. \tag{1}$$

Here $N_{\mathrm{up}}$ and $N_{\mathrm{down}}$ are the counts registered by the up and down telescopes respectively, $A_\beta$ is the asymmetry parameter determined by the $\beta$ decay under consideration, and $P$ is the amount of spin polarization. $Q_{\mathrm{exp}}$ takes into account the experimental asymmetry losses due to, for instance, the relaxation, the scattering of $\beta$ particles, the experimental geometry, and so on.

In the first order perturbation theory, the transition frequency between the magnetic substates $m$ and $m+1$ of a nuclear spin $I$ under the combined Zeeman and electric quadrupole interactions is given by [47]

$$\nu_m - \nu_{m+1} = \nu_L - \nu_Q \frac{3(3\cos^2\theta - 1)(2m+1)}{8I(2I-1)}. \tag{2}$$

Here $\nu_L$ denotes the Larmor frequency $\nu_L = g\mu_N B_0/h$, $\nu_Q$ the quadrupole coupling constant $\nu_Q = eQ_sV_{zz}/h$, and $\theta$ the angle between the external field $B_0$ and the symmetry axis of the electric field gradient (EFG) $V_{zz}$ of the crystal. Depending on the mounted crystal and applied rf field, one can deduce either the $g$ factor or the quadrupole moment of a nuclear state, by measuring the corresponding transition frequencies between magnetic substates.

For the $g$-factor measurement, nuclei are implanted into a Si crystal with cubic lattice structure (zero EFG) so that the second term on the right-hand side of Eq. (2) vanishes. The magnetic substates of nuclear spins $I$ under such circumstance split equally in energy with $E_m - E_{m+1} = h\nu_L$. When the applied rf frequency $\nu_{\mathrm{RF}}$ matches the Larmor frequency $\nu_L$, the transition between two neighboring magnetic substates is resonant, and the ensemble polarization is destroyed. This results in a resonant change in the $\beta$-decay asymmetry $\mathcal{A}$ in the $\beta$-NMR spectrum, from which the Larmor frequency $\nu_L$ can be deduced. In combination with the known static magnetic field $B_0$, this gives access to the $g$ factor. For the quadrupole moment measurement, on the other hand, the nuclei are implanted in a $\alpha$-$Al_2O_3$ crystal with a hexagonal crystal structure, thus inducing an axially symmetric EFG $V_{zz}$. This crystal was mounted such that the symmetry axis of the EFG is parallel to the static magnetic field $B_0$ (thus with $\cos^2\theta = 1$). According to Eq. (2), an $I = 1$ state splits into three substates with two unequal transition frequencies $\nu_L \pm \frac{3}{4}\nu_Q$. The destruction of the $\beta$-decay

**Table 1**
Experimental results of this work. The $g$ factors are extracted with the static field $B_0 = 1501(5)_{\rm sys}$ gauss. The quadrupole moments are obtained using the $^{27}$Al data in the $\alpha$-$Al_2O_3$ crystal as a reference. The half life of $^{34m}$Al is taken from Ref. [42]. The literature values of the $g$ factor and $Q_s$ of $^{32}$Al are from Refs. [39] and [37], respectively. See text for more information.

| | $N$ | $I^\pi$ | $T_{1/2}$ | $g$ factor | | | $Q_s$ (mb) | | |
|---|---|---|---|---|---|---|---|---|---|
| | | | | $\nu_L$ (kHz) | This work | Lit. | $\nu_Q$ (kHz) | This work | Lit. |
| $^{32}$Al | 19 | $1^+$ | 33.0 ms | 2240.5(7) | $1.958(1)(7)_{\rm sys}$ | 1.9516(22) | 418(4) | 25.5(3) | 24(2) |
| $^{34m}$Al | 21 | $1^+$ | 26 ms | $2010 \pm 15$ | $1.757 \pm 0.014$ | | 627(83) | 38(5) | |

asymmetry is maximized by simultaneously applying two rf frequencies equal to these two transition frequencies respectively. These frequencies are varied simultaneously as a function of $\nu_Q$. In practical, it is necessary to know the Larmor frequency in advance so that the two rf frequencies applied to nuclei are set to $\nu_{\rm RF}^{\pm} = \nu_L \pm \Delta$. By scanning $\Delta$, a resonance signal in asymmetry $\mathcal{A}$ is observed if the condition $\Delta = \frac{3}{4}\nu_Q$ is matched. In both NMR and NQR measurements, the rf frequencies are scanned in several discrete steps. To cover the frequency range in between the steps, a frequency modulation of more than 50% of the step size is applied. More technical details of the experimental setup and method can be found in Ref. [46].

Prior to the $^{34m}$Al measurements, the experimental setup was optimized using the $^{32}$Al isotope, of which the $g$ factor and quadrupole moment are well known [36,37,39]. The results are summarized in Table 1.

The $\beta$-NMR spectra showing the experimental $\beta$-decay asymmetry as a function of the applied rf frequency in a Si crystal are plotted in Fig. 1 for $^{32}$Al (top) and $^{34m}$Al (middle and bottom). Note that for $^{34m}$Al the change in asymmetry is negative as expected, opposite to what is seen in $^{32}$Al which has the opposite polarization because of the different production mechanism [45]. A series of measurements with different frequency ranges and frequency modulation were carried out for $^{32}$Al to verify the experimental setup and confirm the literature values from previous works. The spectra from each measurement were fitted using a Lorentzian function, of which the amplitude, centroid frequency, baseline, and linewidth are free to fit. The Larmor frequency, $\nu_L(^{32}\text{Al}) = 2240.5(7)$ kHz, has been determined from the weighted average of different runs. With a calibrated magnetic field of $B_0 = 1501(5)_{\rm sys}$ gauss, the $g$ factor of $^{32}$Al is deduced to be $|g| = 1.958(1)(7)_{\rm sys}$, consistent with the literature value as shown in Table 1. In contrast, the $^{34m}$Al measurement suffered from several difficulties. First of all, the total production rate of $^{34}$Al was measured to be a factor of 20 less than that of $^{32}$Al at the same primary-beam intensity. Additionally, the yield of the isomer in $^{34}$Al is even further reduced as the isomer-to-ground state ratio is estimated to lie between 30% and 70%. Due to the $^{34}$Al daughter and grand-daughter activities, approximately only one third of the detected $\beta$ particles are associated to $^{34}$Al and only 30–70% of those to the isomer. The amplitude of the experimentally observed asymmetry is therefore significantly reduced, as confirmed by simulations. While the daughter and grand-daughter decays can be partly cut out based on their significantly lower $\beta$ energies (at the cost of reducing the statistics on $^{34m}$Al), this is not applicable for the ground-state decays due to the similar $\beta$-decay $Q_\beta$ value as that of the isomer. The combination of a low yield with a small-amplitude signal made the measurements extremely challenging. Only the broad frequency scans with few steps (60 kHz step size and 45 kHz modulation) provided high enough statistics to observe the signal. As shown in Fig. 1 (middle), no resonance is seen for $^{34m}$Al, and there is a single point at $\nu_{\rm RF} = 2010$ kHz having a significant deviation from the weighted average baseline (indicated by the horizontal line). This is due to the very broad frequency modulation that was used to search for the resonance

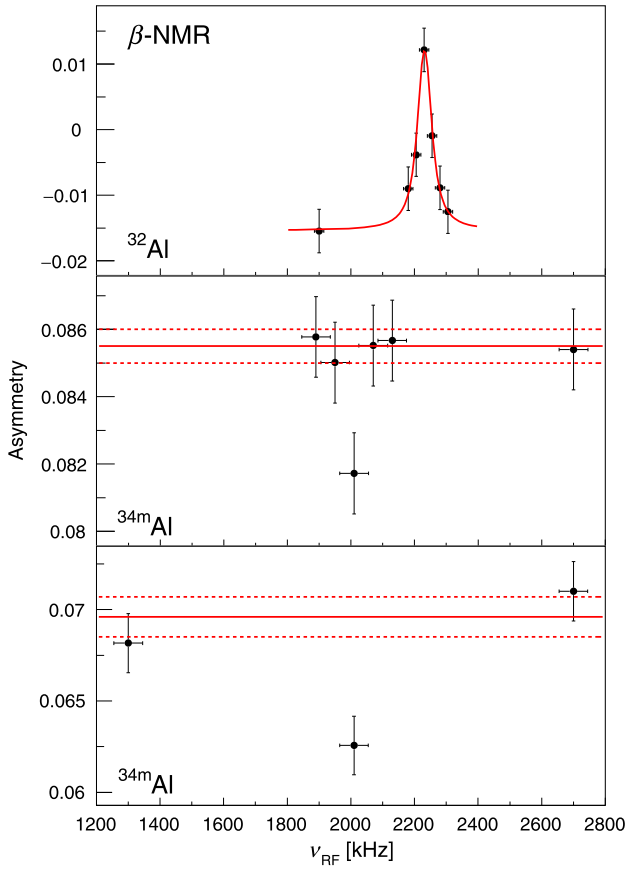


**Fig. 1.** The $\beta$-decay asymmetry $\mathcal{A}$ in the Si crystal as a function of applied rf frequency $\nu_{\rm RF}$ (kHz) for $^{32}$Al (top) and $^{34m}$Al (middle and bottom). The polarization orientation is different between the two isotopes due to the different production mechanics. The sizes of horizontal error bars correspond to the amplitudes of frequency modulation, which are 15 and 45 kHz for $^{32}$Al and $^{34m}$Al, respectively. The $^{32}$Al spectrum is fitted by a Lorentzian lineshape (red curve), while only the averaged baseline with its variation is drawn for the $^{34m}$Al spectra. See text for more explanation. (For interpretation of the colors in the figure(s), the reader is referred to the web version of this article.)

signal. Since the asymmetry on both sides of the 2010-kHz point is that of the baseline, the Larmor frequency of $^{34m}$Al cannot lie within the $1950 \pm 45$ kHz nor $2070 \pm 45$ kHz ranges, thus it has to be in the range of $2010 \pm 15$ kHz. The corresponding $g$ factor, $|g(^{34m}\text{Al})|$, is determined as $1.757 \pm 0.014$, where the symbol "$\pm$" indicates the range in which the observable lies, as outlined above. The same notation is used throughout the paper. Note that because the applied frequency modulation range is very large, no meaningful $1\sigma$ statistical error can be deduced for the Larmor frequency. All frequencies in the determined range have equal probability to be the Larmor frequency.

However, the signal shown in Fig. 1 (middle) only has a $2.8\sigma$ deviation from the baseline, where $\sigma$ is the root sum square of the baseline variation and the asymmetry uncertainty at 2010 kHz.

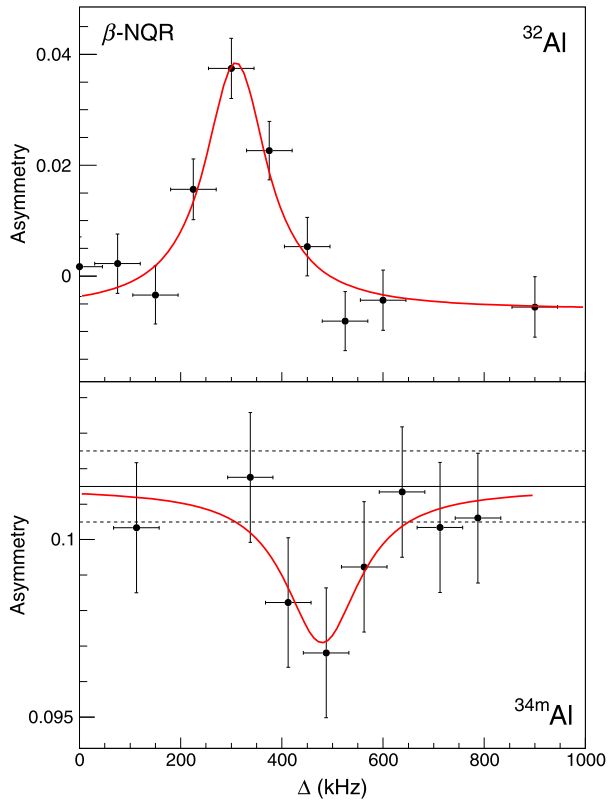


**Fig. 2.** The $\beta$-decay asymmetry $\mathcal{A}$ in the $\alpha$-$Al_2O_3$ crystal as a function of $\Delta$ (kHz) for $^{32}$Al (top) and $^{34m}$Al (bottom). The applied rf frequencies are $\nu_{RF}^{\pm} = \nu_L \pm \Delta$, in which the Larmor frequencies are 2240 and 2020 kHz for $^{32}$Al and $^{34}$Al respectively. The polarization orientation is different between the two isotopes due to the different production mechanics. The sizes of horizontal error bars correspond to the amplitudes of frequency modulation, which are 45 kHz for both $^{32}$Al and $^{34}$Al. Both spectra are fitted by a Lorentzian lineshape shown as the red curve. The baseline and its variation (determined from the fit) of the $^{34m}$Al spectrum are drawn as a reference.

To further consolidate the observed signal, a second scan exclusively focusing on the single resonance and two satellite points was performed, with the same frequency modulation (45 kHz) as the former scan. The asymmetry of the two satellite points at 1300 and 2700 kHz was used to determine the averaged baseline, see Fig. 1 (bottom). The asymmetry change at resonance is now more than $3.5\sigma$, reducing the probability that the deviation is purely statistical to less than $5 \times 10^{-4}$.

In the $\beta$-NQR measurement of $^{34m}$Al, the asymmetry parameter $\mathcal{A}$ was scanned as a function of $\Delta$ with frequency modulation 45 kHz and step size 60 kHz. The spectrum is plotted in Fig. 2 (bottom), together with that of $^{32}$Al (top) measured under the same experimental conditions. The Larmor frequencies in the $\beta$-NQR scans of $^{32}$Al and $^{34m}$Al are fixed at 2240 and 2020 kHz respectively. Although for $^{34m}$Al there could be a difference between the applied and the real Larmor frequency (within our quoted uncertainty), it has been demonstrated previously [48] and verified with $^{32}$Al in this work, that this does not affect the extracted $\nu_Q$. A slightly shifted $\nu_L$ value would make the resonance a little broader but would not alter the central frequency of $\Delta$. However, as our modulation range is much larger than the uncertainty on $\nu_L$, this will not have an influence here. It is noted that a very clear NQR resonance seen here also proves that our NMR-resonance is correct, since a resonance can only be observed if the Larmor frequency (the $g$ factor) is properly measured and set during the multiple-RF NQR scan. A Lorentzian function is employed to fit the

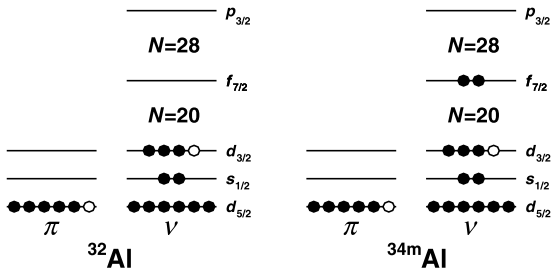


**Fig. 3.** Proposed proton ($\pi$) and neutron ($\nu$) leading configurations in the $1^+$ state of $^{32}$Al (left) and $^{34m}$Al (right). Particles and holes are presented by solid and open circles respectively.

NQR resonance to extract $\nu_Q$ from each measurement. For $^{32}$Al, a weighted mean value of four runs with different modulation and step size gives $\nu_Q = 418(4)$ kHz. To fit the spectrum of $^{34m}$Al, the linewidth of the resonance is fixed to the value determined from $^{32}$Al, as the same modulation and rf power where used. Following this analysis, $\nu_Q = 627(83)$ kHz is obtained for $^{34m}$Al. From the definition of $\nu_Q$, one finds

$$\frac{\nu_Q(^A\mathrm{Al})}{|Q_s(^A\mathrm{Al})|} = \frac{eV_{zz}}{h} \tag{3}$$

to be constant for various mass numbers $A$ in the same crystal. Using $^{27}$Al as a reference, of which $Q_s = +146.6(10)$ mb and $\nu_Q = 2403.1(2)$ kHz have been measured in $\alpha$-$Al_2O_3$ at room temperature [49,50], quadrupole moments of 25.5(3) and 38(5) mb are extracted for $^{32}$Al and $^{34m}$Al, respectively. The static quadrupole moment of $^{32}$Al measured in this work is an order of magnitude more precise than the earlier reported value [37].

According to the shell-model and $\beta$ decay studies of $^{34}$Al, the $1^+$ isomer is proposed to be a $1p1h$ intruder state with respect to $N = 20$ [22,42]. A schematic drawing of this configuration, $\pi(d_{5/2})^{-1} \otimes \nu(d_{3/2})^{-1}(f_{7/2})^2$, is illustrated in Fig. 3 (right), in comparison with the leading configuration of the $^{32}$Al ground state (left). Since the nuclear $g$ factor (related to the magnetic moment $\mu = gI\mu_N$) is very sensitive to the orbits occupied by unpaired nucleons, it provides a stringent test for the validity of the proposed configuration. In case most of the two $pf$-shell neutrons in $^{34m}$Al couple to spin $J = 0$, they act as "spectators" that do not contribute to the magnetic moment. In this case, we expect the $^{34m}$Al and $^{32}$Al $g$ factors to be similar, which is indeed the case. Their values can also be compared to the Schmidt moment for a $(\pi d_{5/2} \otimes \nu d_{3/2})_{I=1}$ configuration. Indeed, in a simple single-particle model, the $g$ factor of a nuclear state with total spin $I$ can be described by a weak coupling between protons and neutrons, resulting in [44]

$$g(I) = \frac{1}{2}\left[(g_\pi + g_\nu) + (g_\pi - g_\nu)\frac{I_\pi(I_\pi+1) - I_\nu(I_\nu+1)}{I(I+1)}\right], \tag{4}$$

where $g_{\pi(\nu)}$ is the proton (neutron) $g$ factor. If the Schmidt values are used here with the proposed configuration, we get $g_{\mathrm{sch}}(^{32}\mathrm{Al}) = g_{\mathrm{sch}}(^{34m}\mathrm{Al}) = 2.78$, well above the observed values. That is due to missing nucleon correlations. These can be accounted for to some extent by using the experimental $g$ factors of the near-by odd-mass isotopes. Using the known $g$ factors of $^{31}$Al and $^{33}$Al for the $\pi d_{5/2}$ configuration, and that of $^{33}$Si for the $\nu d_{3/2}$ configuration [51], we obtained respectively $g(^{32}\mathrm{Al}) = 2.08$ and $g(^{34m}\mathrm{Al}) = 2.28$, closer to the observed values. Thus the intuitive picture confirms the $1p1h$ nature of the isomer which was proposed based on the

**Table 2**
Available experimental $g$ factors and quadrupole moments of $^{32-34}$Al compared with shell-model calculations using the SDPF-U-MIX (denoted as MIX) [10], SDPF-M [52], and EEdf1 [53] interactions. Experimental data denoted by * is derived from the present work. Calculated $g$ factors are obtained using free nucleon $g$ factors, while quadrupole moments are calculated using effective charges $(e_\pi, e_\nu) = (1.1e, 0.5e)$. The EEdf1 results of $^{34m}$Al include both the $1^+_1$ and $1^+_2$ states. See text for more information.

| | $I^\pi$ | $g$ factor | | | | $Q_s$ (mb) | | | |
|---|---|---|---|---|---|---|---|---|---|
| | | Exp | MIX | SDPF-M | EEdf1 | Exp | MIX | SDPF-M | EEdf1 |
| $^{32}$Al | $1^+$ | 1.9516(22) [39] | 1.80 | 1.83 | – | 25.5(3)* | 23.2 | 25.6 | – |
| $^{33}$Al | 5/2+ | 1.635(2) [39] | 1.67 | 1.55 | – | 141(3) [41] | 113.2 | 152.8 | – |
| $^{34g}$Al | $4^-$ | 0.539(2) [22] | 0.54 | 0.41 | 0.55 | – | 46.3 | 76.1 | 237.9 |
| $^{34m}$Al | $1^+$ | $1.757 \pm 0.014$* | 1.76 | 1.73 | 0.14 ($1^+_1$) | 38(5)* | 41.5 | 39.6 | 79.0 ($1^+_1$) |
| | | | | | 1.52 ($1^+_2$) | | | | 35.6 ($1^+_2$) |

$\beta$ decay of $^{34}$Al [42]. However, the $g$ factor of $^{34m}$Al also shows a 10% decrease with respect to that of $^{32}$Al, implying a slightly different mixing with configurations other than that of $^{32}$Al in the isomer's wave function.

To take into account more complex wave functions, the measured $g$ factors are compared to large-scale shell-model calculations with different effective interactions. These include two widely used interactions in the island of inversion, SDPF-U-MIX [10] and SDPF-M [52]. In addition, calculations are made with a new effective interaction, EEdf1, which is purely derived from a realistic nucleon–nucleon potential using the extended Kuo-Krenciglowa method [53]. This interaction has been successfully employed to study the Ne, Mg, and Si isotopes with $N \sim 20$ [53,54], and is applied to $^{34}$Al in this work. All three interactions are constructed based on a $^{16}$O core. While SDPF-M considers only the $f_{7/2}$ and $p_{3/2}$ orbits on top of the $sd$ shell, SDPF-U-MIX and EEdf1 include the full $sd + pf$ shells in their model space. To reduce the computation time, particle-hole excitations are limited up to $4p4h$ in all calculations. As in our previous work in this mass region [20,22,39], the $g$ factors are calculated using free nucleon single-particle $g$ factors. The calculated $g$ factors are compared in Table 2. SDPF-M and SDPF-U-MIX give a very similar $g$ factor for $^{34m}$Al which is in good agreement with experiment and as suggested by our simple calculations in previous paragraph, its predicted wave function is dominated by $1p1h$ configuration. In the EEdf1 interaction, two $1^+$ states are calculated within less than 150 keV. Since EEdf1 is free from any fit of two-body matrix elements, calculation precision is a few hundred keV and hence both states should be considered. The lowest $1^+$ state is predicted to be mainly dominated by $3p3h$ configurations ($\sim 75\%$) and its $g$ factor is an order of magnitude smaller than the experimental ones. This excludes a $3p3h$ configuration for the $1^+$ isomer. However, the $1^+_2$ state has a mixed $1p1h$ and $3p3h$ configuration ($\sim 50\%$ for each) with a $g$ factor that is much closer to the experimental value. This confirms the conclusions from the SDPF-U-MIX and SDPF-M calculations which reproduce the experimental $g$ factor very well and predict a dominating $1p1h$ nature of the observed isomer.

Next we have a look at the quadrupole moments. In spite of their similar $g$ factors, the experimental quadrupole moment of $^{34m}$Al shows an increase in amplitude of 50% with respect to that of $^{32}$Al, indicating the isomer is more deformed than $^{32}$Al. In Table 2, the experimental data is compared with the calculations obtained using proton and neutron effective charges $(e_\pi, e_\nu) = (1.1e, 0.5e)$, which have been suggested based on the systematic study of quadrupole moments in the proton $sd$-shell nuclei [38]. As shown in the table, calculated quadrupole moments using all three interactions (take $1^+_2$ from EEdf1) agree well with the experimental data of $^{34m}$Al. Moreover, both SDPF-M and SDPF-U-MIX nicely reproduce the increasing trend of $Q_s(1^+)$ from $A = 32$ to 34. In SDPF-M, an examination on the respective proton and neutron contributions reveals that the enhancement is mainly due to the neutrons occupying the $\nu f_{7/2}$ orbit above $N = 20$. Since a neutron $J = 0$ pair does not contribute to quadrupole moment, it suggests a sizable component with $(\nu f^2_{7/2})_{J\geq 2}$ mixed in the isomeric state. This can also explain the variation of $g$ factor between $^{34m}$Al and $^{32}$Al, though the quadrupole moment is much more sensitive to this component than the $g$ factor. As discussed previously, the lowest $1^+$ state in EEdf1 overestimates the quadrupole moment (79 mb) due to the too strong $3p3h$ excitations. Again, the second $1^+$ state gives a much more reasonable result compared with the experimental data.

As discussed above, SDPF-U-MIX and SDPF-M give very similar results for $^{34m}$Al while for some cases in the past, clear discrepancies between different shell-model interactions were observed. To better understand the differences between the interactions and how those affect the nuclear moments, it is therefore instructive to give a short overview of the available information of Al isotopes near or inside the island of inversion. As $^{32}$Al is considered to lie outside of the island of inversion, the $g$ factors and quadrupole moments of SDPF-U-MIX and SDPF-M are very similar and close to the USD predictions [55]. The small underestimation of a few percent in the $g$ factor is understood as a consequence of overestimating the proton $\pi d_{3/2}$ component in the calculated wave function [39]. $^{33}$Al at $N = 20$ is considered the transition point into the island, at least from the nuclear moments point of view. Historically, the small but uncharacteristic deviation of a few percent from the USD calculated $g$ factor was the first indication of the mixed normal-intruder nature of the ground state [22]. The more sophisticated SDPF-U-MIX and SDPF-M interactions predict very different wave functions for $^{33}$Al, with 17% and 74% of intruder admixtures respectively [41], but their calculated $g$ factors are quite similar. The experimental value lies in between these two predictions, showing somewhat better agreement with the SDPF-U-MIX value. However, the ground-state quadrupole moment is much more sensitive to the amount of intruder configurations. While the SDPF-U-MIX and USD interactions predicts a decline in quadrupole moment from $^{31}$Al ($N = 18$) to $^{33}$Al, only the SDPF-M interaction reproduces the rising trend observed experimentally. The discrepancy between SDPF-U-MIX predictions and experimental data was suggested to arise from the underestimation of the intruder configurations and thus from a too strong $N = 20$ gap. Moving to $^{34}$Al, the ground-state $g$ factor is well consistent with the SDPF-U-MIX and EEdf1 calculations, which manifest stronger neutron excitations across the $N = 28$ gap (between the $\nu f_{7/2}$ and $\nu p_{3/2}$ orbits) than that in SDPF-M. The latter shows a sizable deviation over 20% from the literature value, which can be improved by the interplay of decreasing the $N = 20$ and $N = 28$ shell gaps. This has been verified using the SDPF-M' interaction, of which the $N = 28$ gap is reduced by 500 keV with respect to that of SDPF-M [22]. Due to the increased $p_{3/2}$ occupancy, the ground-state $g$ factor of SDPF-M' (0.478) agrees better with the experimental data, and the state becomes an intruder state with 55% contribution from $2p2h$ excitations. It is interesting to note that in EEdf1 the $4^-_1$ state is also an intruder state, dominated by

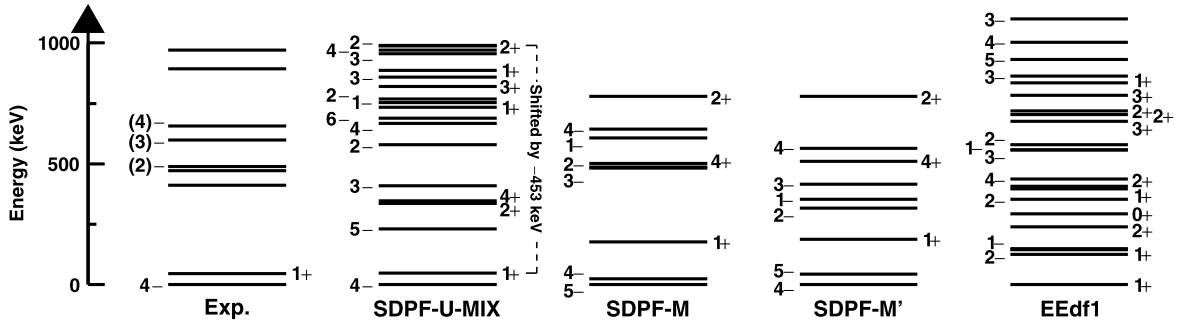


**Fig. 4.** The level schemes of $^{34}$Al below 1 MeV. Experimental data is taken from Refs. [43,56]. The level schemes calculated by SDPF-U-MIX and SDPF-M/SDPF-M' are taken from Refs. [22,43]. The positive-parity states given by SDPF-U-MIX are shifted downwards by 453 keV systematically. See text for more information for the calculations.

$2p2h$ ($\sim 70\%$) configurations. The corresponding quadrupole moment is thus significantly larger than that of either SDPF-U-MIX or SDPF-M. To fully identify the configuration of the ground state and to constrain different theoretical calculations, it is of great interest to measure this quadrupole moment in a dedicated experiment in the future.

Finally, the level schemes from those shell-model calculations are compared. The calculated results below 1 MeV are summarized in Fig. 4, together with the experimental data taken from [43,56]. For a discussion like this, one can not forget that an uncertainty of a few hundred keV on the calculated energy levels of complex odd–odd nuclei like $^{34}$Al is to be expected for any of the interactions. As such, the overall agreement between theory and experiment is quite limited. Nevertheless, a few interesting conclusions can be drawn. The excitation energies calculated using SDPF-U-MIX are taken from Ref. [43]. In order to match the relative energy splitting between $4^-$ and $1^+$, positive-parity levels were shifted downwards systematically by 453 keV. Since the excitation energy of the intruder $1^+$ state is very sensitive to the size of the $N = 20$ gap, it again points towards an overestimated $N = 20$ shell gap at $Z = 13$, as inferred from the $^{33}$Al quadrupole moment. The levels calculated by SDPF-M are taken from Ref. [22]. Note that the calculation was performed using the Monte Carlo Shell Model [57] without restrictions on the amount of particle-hole excitations. In this case, the $1^+$ state is naturally given as an isomer. However, the interaction predicts a $5^-$ ground state, while the $4^-$ state is 20 keV above. As suggested by Ref. [22], reducing the $N = 28$ shell gap (as SDPF-M') is applicable to reproduce correctly the ground-state spin. Generally EEdf1 seems to behave the worst: the lowest $1^+$ state does not correspond to the $1^+$ isomer, and the experimental ground state $4^-$ is given around 400 keV higher. Considering the calculated $g$ factors or quadrupole moments for the lowest $4^-$ and second $1^+$ states reasonably agree with the available experimental data, the wave functions given by EEdf1 seem to be correct. The discrepancy in excitation energies might arise from the choice of single-particle energies. For instance, if the single-particle energies above $N = 20$ are too low, $3p3h$ excitations will be overwhelming in the lowest $1^+$ state. Further investigation is required to improve its predictive power on excitation energies for odd–odd nuclei.

In conclusion, the properties of the Al isotopes are quite sensitive to the $N = 20$ and $N = 28$ shell gaps in each interaction. As not every isotope and observable is sensitive to the same effects, measurements on a wide variety of properties in the region is necessary to assess the available theories as well as to offer clues for their improvements.

In summary, the $g$ factor and quadrupole moment of $^{34m}$Al have been measured using the $\beta$-NMR/NQR techniques at GANIL with an estimated isomeric production rate of less than 300 ions/s. The Larmor frequency of $^{34m}$Al was observed within the range $2010 \pm 15$ kHz in a $1501(5)_{\text{sys}}$-gauss static field, yielding $|g(^{34m}\text{Al})|$ within $1.757 \pm 0.014$. The quadrupole coupling constant of $^{34m}$Al was deduced at $\nu_Q = 627(83)$ kHz in a $\alpha$-$Al_2O_3$ crystal, which corresponds to $|Q_s(^{34m}\text{Al})| = 38(5)$ mb. The newly measured $g$ factor of $^{34m}$Al is close to that of $^{32}$Al, which can be attributed to very similar orbital occupations of the odd proton and neutron. This, together with the comparison with empirical $g$ factors calculated from simple proton–neutron coupling scheme, establishes firmly the $1p1h$ nature of the isomer. The quadrupole moment of $^{34m}$Al increases about 50% in amplitude with respect to that of $^{32}$Al, evidencing the enhanced deformation due to the particle-hole excitation across $N = 20$.

The experimental data was compared to large-scale shell-model calculations using several effective interactions. SDPF-M and SDPF-U-MIX well reproduce the measured moments, while in the EEdf1 calculations it is rather the second $1^+$ state which seems to correspond to the observed isomer. This comparison corroborates a wave function dominated by $1p1h$ configurations in the isomer, and excludes a large admixture with $3p3h$ configurations. Together with the moments of $^{32-34}$Al and the energy levels of $^{34}$Al, the status of these interactions at the boundary of the island of inversion is reviewed.

## Acknowledgements

The authors thank the GANIL staff for their support during the preparation and running of the experiment. This work was partly supported by the European Union's Horizon 2020 research and innovation programme under grant agreement No. 654002, by the FWO-Vlaanderen, by the IAP programme of the Belgium Science Policy under Grants No. P6/23 and No. P7/12, by the Nupnet network SARFEN (PRI-PIMMNUP-2011-1361), by MINECO (Spain) grant FPA2014-57196, by programa Severo Ochoa SEV-2016-0597, by Grants-in-Aid for Scientific Research (23244049, 15K05090), by the HPCI Strategic Program (hp140210, hp150224), by MEXT and JICFuS as a priority issue (Elucidation of the fundamental laws and evolution of the universe) to be tackled by using Post "K" Computer (hp160211), by the CNS-RIKEN joint project for large-scale nuclear structure calculations. The experiment was carried out under Experimental Program E650.

## References

[1] O. Haxel, J.H.D. Jensen, H.E. Suess, On the "magic numbers" in nuclear structure, Phys. Rev. 75 (1949) 1766.
[2] M.G. Mayer, On closed shells in nuclei. II, Phys. Rev. 75 (1949) 1969–1970.
[3] O. Sorlin, M.-G. Porquet, Nuclear magic numbers: new features far from stability, Prog. Part. Nucl. Phys. 61 (2008) 602–673.
[4] E.K. Warburton, J.A. Becker, B.A. Brown, Mass systematics for $A = 29$–$44$ nuclei: the deformed $A \sim 32$ region, Phys. Rev. C 41 (1990) 1147–1166.
[5] C. Thibault, R. Klapisch, C. Rigaud, A.M. Poskanzer, R. Prieels, L. Lessard, W. Reisdorf, Direct measurement of the masses of $^{11}$Li and $^{26-32}$Na with an on-line mass spectrometer, Phys. Rev. C 12 (1975) 644–657.

[6] G. Huber, F. Touchard, S. Büttgenbach, C. Thibault, R. Klapisch, H.T. Duong, S. Liberman, J. Pinard, J.L. Vialle, P. Juncar, et al., Spins, magnetic moments, and isotope shifts of $^{21-31}$Na by high resolution laser spectroscopy of the atomic $D_1$ line, Phys. Rev. C 18 (1978) 2342–2354.

[7] C. Détraz, D. Guillemaud, G. Huber, R. Klapisch, M. Langevin, F. Naulin, C. Thibault, L.C. Carraz, F. Touchard, Beta decay of $^{27-32}$Na and their descendants, Phys. Rev. C 19 (1979) 164–176.

[8] A. Poves, J. Retamosa, The onset of deformation at $N = 20$ neutron shell closure far from stability, Phys. Lett. B 184 (1987) 311–315.

[9] T. Otsuka, T. Suzuki, M. Honma, Y. Utsuno, N. Tsunoda, K. Tsukiyama, M. Hjorth-Jensen, Novel features of nuclear forces and shell evolution in exotic nuclei, Phys. Rev. Lett. 104 (2010) 012501.

[10] E. Caurier, F. Nowacki, A. Poves, Merging of the islands of inversion at $N = 20$ and $N = 28$, Phys. Rev. C 90 (2014) 014302.

[11] D. Guillemaud-Mueller, C. Detraz, M. Langevin, F. Naulin, M. de Saint-Simon, C. Thibault, F. Touchard, M. Epherre, $\beta$-decay schemes of very neutron-rich sodium isotopes and their descendants, Nucl. Phys. A 426 (1984) 37–76.

[12] P. Baumann, A. Huck, G. Klotz, A. Knipper, G. Walter, G. Marguier, H. Ravn, C. Richard-Serre, A. Poves, J. Retamosa, $^{34}$Si: a new doubly magic nucleus?, Phys. Lett. B 228 (1989) 458–462.

[13] T. Motobayashi, Y. Ikeda, K. Ieki, M. Inoue, N. Iwasa, T. Kikuchi, M. Kurokawa, S. Moriya, S. Ogawa, H. Murakami, et al., Large deformation of the very neutron-rich nucleus $^{32}$Mg from intermediate-energy coulomb excitation, Phys. Lett. B 346 (1995) 9–14.

[14] H. Iwasaki, T. Motobayashi, H. Sakurai, K. Yoneda, T. Gomi, N. Aoi, N. Fukuda, Z. Fülöp, U. Futakami, Z. Gacsi, et al., Large collectivity of $^{34}$Mg, Phys. Lett. B 522 (2001) 227–232.

[15] B.V. Pritychenko, T. Glasmacher, B.A. Brown, P.D. Cottle, R.W. Ibbotson, K.W. Kemper, L.A. Riley, H. Scheit, First observation of an excited state in the neutron-rich nucleus $^{31}$Na, Phys. Rev. C 63 (2000) 011305.

[16] Y. Yanagisawa, M. Notani, H. Sakurai, M. Kunibu, H. Akiyoshi, N. Aoi, H. Baba, K. Demichi, N. Fukuda, H. Hasegawa, et al., The first excited state of $^{30}$Ne studied by proton inelastic scattering in reversed kinematics, Phys. Lett. B 566 (2003) 84–89.

[17] P. Doornenbal, H. Scheit, N. Aoi, S. Takeuchi, K. Li, E. Takeshita, H. Wang, H. Baba, S. Deguchi, N. Fukuda, et al., Spectroscopy of $^{32}$Ne and the "island of inversion", Phys. Rev. Lett. 103 (2009) 032501.

[18] P. Doornenbal, H. Scheit, N. Kobayashi, N. Aoi, S. Takeuchi, K. Li, E. Takeshita, Y. Togano, H. Wang, S. Deguchi, et al., Exploring the "island of inversion" by in-beam $\gamma$-ray spectroscopy of the neutron-rich sodium isotopes $^{31,32,33}$Na, Phys. Rev. C 81 (2010) 041305.

[19] P. Doornenbal, H. Scheit, S. Takeuchi, N. Aoi, K. Li, M. Matsushita, D. Steppenbeck, H. Wang, H. Baba, H. Crawford, et al., In-beam $\gamma$-ray spectroscopy of $^{34,36,38}$Mg: merging the $N = 20$ and $N = 28$ shell quenching, Phys. Rev. Lett. 111 (2013) 212502.

[20] G. Neyens, M. Kowalska, D. Yordanov, K. Blaum, P. Himpe, P. Lievens, S. Mallion, R. Neugart, N. Vermeulen, Y. Utsuno, et al., Measurement of the spin and magnetic moment of $^{31}$Mg: evidence for a strongly deformed intruder ground state, Phys. Rev. Lett. 94 (2005) 022501.

[21] D.T. Yordanov, M. Kowalska, K. Blaum, M. De Rydt, K.T. Flanagan, P. Lievens, R. Neugart, G. Neyens, H.H. Stroke, Spin and magnetic moment of $^{33}$Mg: evidence for a negative-parity intruder ground state, Phys. Rev. Lett. 99 (2007) 212501.

[22] P. Himpe, G. Neyens, D. Balabanski, G. Bélier, J. Daugas, F. de Oliveira Santos, M.D. Rydt, K. Flanagan, I. Matea, P. Morel, et al., $g$ factor of the exotic $N = 21$ isotope $^{34}$Al: probing the $N = 20$ and $N = 28$ shell gaps at the border of the "island of inversion", Phys. Lett. B 658 (2008) 203–208.

[23] R. Kanungo, C. Nociforo, A. Prochazka, Y. Utsuno, T. Aumann, D. Boutin, D. Cortina-Gil, B. Davids, M. Diakaki, F. Farinon, et al., Structure of $^{33}$Mg sheds new light on the $N = 20$ island of inversion, Phys. Lett. B 685 (2010) 253–257.

[24] G. Neyens, Multiparticle-multihole states in $^{31}$Mg and $^{33}$Mg: a critical evaluation, Phys. Rev. C 84 (2011) 064310.

[25] D.T. Yordanov, M.L. Bissell, K. Blaum, M. De Rydt, C. Geppert, M. Kowalska, J. Krämer, K. Kreim, A. Krieger, P. Lievens, et al., Nuclear charge radii of $^{21-32}$Mg, Phys. Rev. Lett. 108 (2012) 042504.

[26] R.W. Ibbotson, T. Glasmacher, B.A. Brown, L. Chen, M.J. Chromik, P.D. Cottle, M. Fauerbach, K.W. Kemper, D.J. Morrissey, H. Scheit, et al., Quadrupole collectivity in $^{32,34,36,38}$Si and the $N = 20$ shell closure, Phys. Rev. Lett. 80 (1998) 2081–2084.

[27] C. Hofmann, J. Reinhardt, W. Greiner, P. Schlüter, G. Soff, Angular correlation of electrons and positrons in internal pair conversion, Phys. Rev. C 42 (1990) 2632–2645.

[28] S. Nummela, F. Nowacki, P. Baumann, E. Caurier, J. Cederkäll, S. Courtin, P. Dessagne, A. Jokinen, A. Knipper, G. Le Scornet, et al., Intruder features in the island of inversion: the case of $^{33}$Mg, Phys. Rev. C 64 (2001) 054313.

[29] W. Mittig, H. Savajols, D. Baiborodin, J. Casandjian, C. Demonchy, P. Roussel-Chomaz, F. Sarazin, Z. Dlouhý, J. Mrazek, A. Belozyorov, et al., Shape coexistence and the $N = 20$ shell closure far from stability by inelastic scattering, Eur. Phys. J. A – Hadrons Nucl. 15 (2002) 157–160.

[30] N. Iwasa, T. Motobayashi, H. Sakurai, H. Akiyoshi, Y. Ando, N. Aoi, H. Baba, N. Fukuda, Z. Fülöp, U. Futakami, et al., In-beam $\gamma$ spectroscopy of $^{34}$Si with deuteron inelastic scattering using reverse kinematics, Phys. Rev. C 67 (2003) 064315.

[31] A. Gade, P. Adrich, D. Bazin, M.D. Bowen, B.A. Brown, C.M. Campbell, J.M. Cook, S. Ettenauer, T. Glasmacher, K.W. Kemper, et al., Spectroscopy of $^{36}$Mg: interplay of normal and intruder configurations at the neutron-rich boundary of the "island of inversion", Phys. Rev. Lett. 99 (2007) 072502.

[32] K. Wimmer, T. Kröll, R. Krücken, V. Bildstein, R. Gernhäuser, B. Bastin, N. Bree, J. Diriken, P. Van Duppen, M. Huyse, et al., Discovery of the shape coexisting $0^+$ state in $^{32}$Mg by a two neutron transfer reaction, Phys. Rev. Lett. 105 (2010) 252501.

[33] N. Hinohara, K. Sato, K. Yoshida, T. Nakatsukasa, M. Matsuo, K. Matsuyanagi, Shape fluctuations in the ground and excited $0^+$ states of $^{30,32,34}$Mg, Phys. Rev. C 84 (2011) 061302.

[34] A.A. Kwiatkowski, C. Andreoiu, J.C. Bale, A. Chaudhuri, U. Chowdhury, S. Malbrunot-Ettenauer, A.T. Gallant, A. Grossheim, G. Gwinner, A. Lennarz, et al., Observation of a crossover of $S_{2n}$ in the island of inversion from precision mass spectrometry, Phys. Rev. C 92 (2015) 061301.

[35] D. Borremans, S. Teughels, N. Smirnova, D. Balabanski, N. Coulier, J.-M. Daugas, F. de Oliveira Santos, G. Georgiev, M. Lewitowicz, I. Matea, et al., Spin and magnetic moment of $^{31}$Al ground state, Phys. Lett. B 537 (2002) 45–50.

[36] H. Ueno, D. Kameda, G. Kijima, K. Asahi, A. Yoshimi, H. Miyoshi, K. Shimada, G. Kato, D. Nagae, S. Emori, et al., Magnetic moments of $^{30}_{13}$Al$_{17}$ and $^{32}_{13}$Al$_{19}$, Phys. Lett. B 615 (2005) 186–192.

[37] D. Kameda, H. Ueno, K. Asahi, D. Nagae, M. Takemura, K. Shimada, A. Yoshimi, T. Nagatomo, T. Sugimoto, M. Uchida, et al., Electric quadrupole moments of neutron-rich nuclei $^{32}$Al and $^{31}$Al, Hyperfine Interact. 180 (2007) 61–64.

[38] M.D. Rydt, G. Neyens, K. Asahi, D. Balabanski, J. Daugas, M. Depuydt, L. Gaudefroy, S. Grévy, Y. Hasama, Y. Ichikawa, et al., Precision measurement of the electric quadrupole moment of $^{31}$Al and determination of the effective proton charge in the $sd$-shell, Phys. Lett. B 678 (2009) 344–349.

[39] P. Himpe, G. Neyens, D. Balabanski, G. Bélier, D. Borremans, J. Daugas, F. de Oliveira Santos, M.D. Rydt, K. Flanagan, G. Georgiev, et al., $g$ factors of $^{31,32,33}$Al: indication for intruder configurations in the $^{33}$Al ground state, Phys. Lett. B 643 (2006) 257–262.

[40] K. Shimada, H. Ueno, G. Neyens, K. Asahi, D. Balabanski, J. Daugas, M. Depuydt, M.D. Rydt, L. Gaudefroy, S. Grévy, et al., Erosion of $N = 20$ shell in $^{33}$Al investigated through the ground-state electric quadrupole moment, Phys. Lett. B 714 (2012) 246–250.

[41] H. Heylen, M. De Rydt, G. Neyens, M.L. Bissell, L. Caceres, R. Chevrier, J.M. Daugas, Y. Ichikawa, Y. Ishibashi, O. Kamalou, et al., High-precision quadrupole moment reveals significant intruder component in $^{33}_{13}$Al$_{20}$ ground state, Phys. Rev. C 94 (2016) 034312.

[42] F. Rotaru, F. Negoita, S. Grévy, J. Mrazek, S. Lukyanov, F. Nowacki, A. Poves, O. Sorlin, C. Borcea, R. Borcea, et al., Unveiling the intruder deformed $0^+_2$ state in $^{34}$Si, Phys. Rev. Lett. 109 (2012) 092503.

[43] R. Lică, F. Rotaru, M.J.G. Borge, S. Grévy, F. Negoiță, A. Poves, O. Sorlin, A.N. Andreyev, R. Borcea, C. Costache, et al., IDS Collaboration, Identification of the crossing point at $N$=21 between normal and intruder configurations, Phys. Rev. C 95 (2017) 021301.

[44] G. Neyens, Nuclear magnetic and quadrupole moments for nuclear structure research on exotic nuclei, Rep. Prog. Phys. 66 (2003) 633.

[45] K. Turzó, P. Himpe, D.L. Balabanski, G. Bélier, D. Borremans, J.M. Daugas, G. Georgiev, F. d, O. Santos, S. Mallion, I. Matea, et al., Spin polarization of $^{34}$Al fragments produced by nucleon pickup at intermediate energies, Phys. Rev. C 73 (2006) 044313.

[46] M.D. Rydt, R. Lozeva, N. Vermeulen, F. de Oliveira Santos, S. Grévy, P. Himpe, C. Stödel, J. Thomas, P. Vingerhoets, G. Neyens, A new dedicated $\beta$-NMR/$\beta$-NQR setup for LISE-GANIL, Nucl. Instrum. Methods Phys. Res., Sect. A, Accel. Spectrom. Detect. Assoc. Equip. 612 (2009) 112–121.

[47] A. Abragam, The Principles of Nuclear Magnetism, International Series of Monographs on Physics, Clarendon Press, 1961.

[48] D. Borremans, Precision Moments of the $^{11}$Li Halo Nucleus, Ph.D. thesis, KU Leuven, 2004.

[49] M.D. Rydt, M. Depuydt, G. Neyens, Evaluation of the ground-state quadrupole moments of the $\pi(sd)$ nuclei, At. Data Nucl. Data Tables 99 (2013) 391–415.

[50] V. Kellö, A.J. Sadlej, P. Pyykkö, D. Sundholm, M. Tokman, Electric quadrupole moment of the $^{27}$Al nucleus: converging results from the AlF and AlCl molecules and the Al atom, Chem. Phys. Lett. 304 (1999) 414–422.

[51] T. Mertzimekis, K. Stamou, A. Psaltis, An online database of nuclear electromagnetic moments, Nucl. Instrum. Methods Phys. Res., Sect. A, Accel. Spectrom. Detect. Assoc. Equip. 807 (2016) 56–60.

[52] Y. Utsuno, T. Otsuka, T. Mizusaki, M. Honma, Varying shell gap and deformation in $N \sim 20$ unstable nuclei studied by the Monte Carlo shell model, Phys. Rev. C 60 (1999) 054315.

[53] N. Tsunoda, T. Otsuka, N. Shimizu, M. Hjorth-Jensen, K. Takayanagi, T. Suzuki, Exotic neutron-rich medium-mass nuclei with realistic nuclear forces, Phys. Rev. C 95 (2017) 021304.

[54] B. Fernández-Domínguez, B. Pietras, W. Catford, N. Orr, M. Petri, M. Chartier, S. Paschalis, N. Patterson, J. Thomas, M. Caamaño, et al., Re-examining the transition into the $N = 20$ island of inversion: structure of $^{30}$Mg, Phys. Lett. B 779 (2018) 124–129.

[55] B.A. Brown, B.H. Wildenthal, Status of the nuclear shell model, Annu. Rev. Nucl. Part. Sci. 38 (1988) 29–66.

[56] B.V. Pritychenko, T. Glasmacher, B.A. Brown, P.D. Cottle, R.W. Ibbotson, K.W. Kemper, H. Scheit, Shape coexistence on the boundary of the "island of inversion": exotic beam spectroscopy of $^{34}$Al, Phys. Rev. C 63 (2001) 047308.

[57] N. Shimizu, T. Abe, Y. Tsunoda, Y. Utsuno, T. Yoshida, T. Mizusaki, M. Honma, T. Otsuka, New-generation Monte Carlo shell model for the K computer era, Prog. Theor. Exp. Phys. 2012 (2012) 01A205.